ChemPubSoc Europe

DOI: 10.1002/cctc.201301055

Rhodium-Complex-Linked Hybrid Biocatalyst: Stereo-Controlled Phenylacetylene Polymerization within an Engineered Protein Cavity

Kazuki Fukumoto,[a] Akira Onoda,[a] Eiichi Mizohata,[a] Marco Bocola,[b] Tsuyoshi Inoue,[a] Ulrich Schwaneberg,[b] and Takashi Hayashi*[a]

The incorporation of a Rh complex with a maleimide moiety into the cavity of the nitrobindin β-barrel scaffold by a covalent linkage at the 96-position (Cys) provides a hybrid biocatalyst that promotes the polymerization of phenylacetylene. The appropriate structural optimization of the cavity by mutagenesis enhances the stereoselectivity of the polymer with a *trans* content of 82% at 25 °C and pH 8.0. The X-ray crystal structure of one of the hybrid biocatalysts at a resolution of 2.0 Å reveals that the Rh complex is located in the β-barrel cavity without any perturbation to the total protein structure. Crystal structure analysis and molecular modeling support the fact that the stereoselectivity is enhanced by the effective control of monomer access to the Rh complex within the limited space of the protein cavity.

Introduction

A hybrid biocatalyst that comprises a synthetic transition metal complex and a well-defined protein scaffold holds promise for the development of homogenous catalysts with new chemical reactivity and selectivity.[1] Hybrid biocatalysts have been constructed through dative,[2] supramolecular,[3] and covalent[4] anchoring approaches to catalyze stereoselective reactions such as hydrogenation,[5] the Diels–Alder reaction,[6] sulfoxidation,[2b,7] and benzannulation.[8] The optimization of the employed protein scaffold by amino acid substitution has often been found to be a powerful strategy to increase the reactivity and enantioselectivity of hydrogenation.[1d,3d,9] One synthetically attractive target will be a new class of hybrid biocatalysts for stereo-controlled C–C bond formation.

This inspired us to prepare a new hybrid biocatalyst that promotes stereo-controlled polymerization within a precisely designed protein cavity. We use acetylene as a monomer because polyacetylene derivatives that consist of valuable π-conjugated polyenes provide useful properties such as electrical conductivity, light emission, and liquid crystallinity.[10] A variety of Rh complexes has been studied as a catalyst for *cis*-selective phenylacetylene polymerization.[11] One example of catalytic phenylacetylene polymerization has been demonstrated within the internal surface of a spherical ferritin cage in which multiple Rh complexes are immobilized.[12] In a separate effort, we have developed a hybrid biocatalyst that contains a mononuclear Rh active site embedded within the robust 10-stranded β-barrel of a heme-free nitrobindin (NB)[13] variant for phenylacetylene polymerization (Figure 1).[14] Interestingly, it was found that the incorporation of the Rh complex into an aponitrobindin variant, NB(Q96C),[15] through a maleimide–thiolate linkage produces an attractive catalyst, NB(Q96C)-**Rh**, which promotes the polymerization of phenylacetylene with approximately 50% *trans* content in the polyphenylacetylene (PPA) (Figure 1). The Rh catalyst without a protein matrix yields *cis*-PPA almost exclusively. To further enhance the *trans*-stereoselectivity of NB(Q96C)-**Rh** in PPA synthesis, the cavity around the Rh active site has been engineered by site-directed mutagenesis. The rigid β-barrel structure of aponitrobindin is able to undergo the computationally guided design of the cavity. In this report,

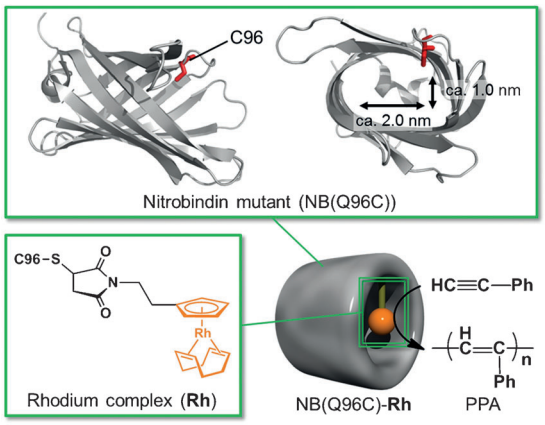

Figure 1. Hybrid biocatalyst NB(Q96C)-**Rh** with a covalently anchored Rh complex within the NB variant (NB(Q96C)), which promotes *trans*-PPA synthesis.

[a] *K. Fukumoto, Dr. A. Onoda, Dr. E. Mizohata, Prof. Dr. T. Inoue, Prof. Dr. T. Hayashi*
Department of Applied Chemistry
Graduate School of engineering, Osaka University
2-1 Yamadaoka, Suita 565-0871 (Japan)
E-mail: thayashi@chem.eng.osaka-u.ac.jp

[b] *Dr. M. Bocola, Prof. Dr. U. Schwaneberg*
Institute of Biotechnology
RWTH Aachen University
Worringerweg 1, 52074 Aachen (Germany)

Supporting information for this article is available on the WWW under http://dx.doi.org/10.1002/cctc.201301055.

we describe the crystal structure and catalysis of the optimized Rh-complex-linked hybrid biocatalyst, which preferentially generates *trans*-PPA.

Results and Discussion

Preparation of hybrid catalysts with a redesigned cavity

To redesign the size and shape of the cavity, we focused on amino acid residues within a distance of 6 Å from the Rh center by using a calculated structure of the prototype hybrid biocatalyst NB(Q96C)-**Rh** (Figure 2a). First, the native His76 and His158 residues, which are closest to the Rh moiety, were replaced with Ala and/or Leu to enlarge the cavity. In addition, one of the six residues Phe44, Leu75, His76, Lys127, Val128, or

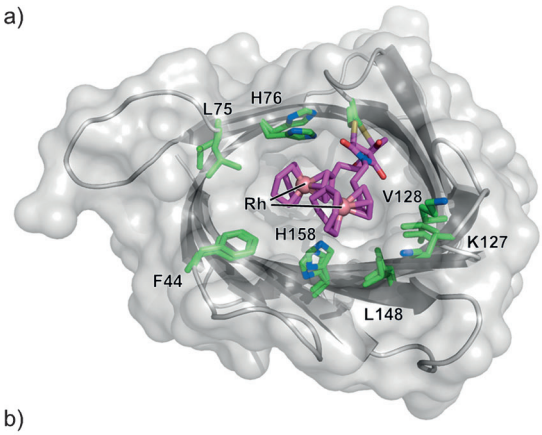

Figure 2. Overview of the ten generated NB variants. a) The amino acid residues in the vicinity of the Rh complex within NB(Q96C)-**Rh**. Two calculated stable conformations of the Rh complex are shown (the Rh atom and its ligand are represented by pink and purple sticks, respectively). Met75 and Met148 were replaced by Leu in all variants. b) List of re-engineered NB variants for stereoselective PPA synthesis.

Leu148 was individually replaced with a Trp residue to increase the tightness of the cavity. Then, a total of ten NB variants that differed in the size and shape of the cavity were designed, produced in *E. coli*, purified, and used as a hybrid protein scaffold (Figure 2b).

Five of the heme-free variants (NB4, NB5, NB6, NB9, and NB10; Figure 2b) were crystallized successfully, and the 3D structures were determined by X-ray crystallography at a resolution of 1.10 –2.20 Å (Figure S2). The re-engineered cavities of the other variants (NB1, NB2, NB3, NB7, and NB8; Figure 2b) in the apo form were evaluated by molecular modeling by using the FoldX plug-in for YASARA software[16] (Figure S3), and the cavity volume of each variant was calculated (Table S3).[17] Notably, the structures of the cavities formed by the robust β-barrel scaffold of NB in all variants are similar to that of the wild type.

NB1-**Rh**-NB10-**Rh** hybrid biocatalysts were prepared by the conjugation of the Rh complex, which contains cyclopentadiene (Cp) and cyclooctadiene (COD) ligands, to each of the freshly reduced variant apoproteins through maleimide coupling to the Cys96 residue. The NB variant (1 mM, 200 μL) was mixed with dithiothreitol (DTT; 2 mg mL^{-1}), and the solution was incubated at 4 °C for 1 h. The reduced protein was purified by using a HiTrap desalting column, which was equilibrated with 10 mM Tris-HCl (pH 7.3). The collected protein solution was diluted to 10 μM with 10 mM Tris-HCl (pH 7.3), and the Rh complex dissolved in DMSO (1 mg/100 μL) was added slowly to the diluted protein solution. The mixed solution was incubated at room temperature for 30 min. The precipitate of the Rh complex was removed by filtration, and the solution was concentrated to 200 μL. The NB variant linked with the Rh complex was purified by using a HiTrap desalting column eluted with 10 mM Tris-HCl buffer (pH 8.0) to remove the unbound Rh complex. All of the conjugates were confirmed by MALDI-TOF MS (Table S4).[18] The amount of attached Rh ions in the NB variants was determined by inductively coupled plasma atomic emission spectroscopy (ICP-OES) and the Bradford assay (Table S4).

Crystal structure of the hybrid catalyst

NB4-**Rh** was purified as follows for X-ray crystal structure analysis: NB4-**Rh** was loaded onto a HiPrep 26/60 Sephacryl S-200 high-resolution column equilibrated with 5 mM MES-HCl buffer (MES = 2-(*N*-morpholino)ethanesulfonic acid; pH 6.0) that contained NaCl (200 mM). The protein fraction was concentrated to 1 mM. NB4-**Rh** was then crystallized by using the hanging-drop vapor diffusion method at 293 K.

The molecular structure of the hybrid biocatalyst NB4-**Rh**, which represents a Rh-linked NB mutant, NB(H76L/Q96C/H158L), was determined by X-ray crystallography at a resolution of 2.0 Å (Figures 3 and S4). The electron density of the Rh complex anchored to the Cys96 residue through the maleimide linker is observed clearly in the $2F_o–F_c$ map, whereas polyethylene glycol (which is used as a precipitant) is found in the cavity of the crystal structure of apo-NB4 without the Rh complex under the same crystallization conditions (Figure 4).[19] According to the crystal structure, the Cp ligand is located in the hydrophobic surface that consists of L100, V128, I131, L148, L158, and L159 residues. The catalytically active Rh center is thus oriented to favor access to the monomer. Notably, the crystal structure correlated well with the structure obtained by the molecular dynamics (MD) simulation data in terms of the position and orientation of the Rh moiety. The root mean standard deviation (RMSD) for the Cα atoms between NB4-**Rh** and the apo-NB4 is 0.27 Å. This indicates that the rigid β-barrel scaffold is retained in the presence of the anchored Rh complex. There is additional support for consistency in the secondary structure of NB4-**Rh** in the results of circular dichroism (CD) measurements. All of the NB hybrids have CD spectra similar to that of the Rh-complex-free proteins (Figures S5 and S6).

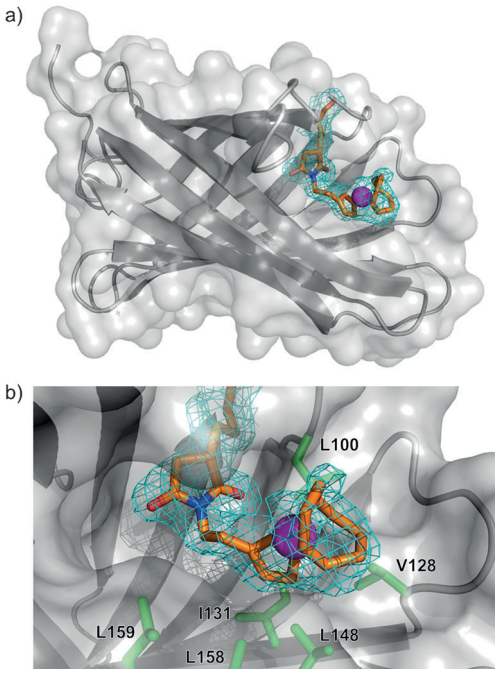

Figure 3. Crystal structure of NB4-**Rh** at a 2.0 Å resolution. a) Whole hybrid catalyst structure and b) close-up views of the covalently linked Rh complex. The $2F_o$–F_c electron density (1.0 σ) and residues in close proximity are also shown.

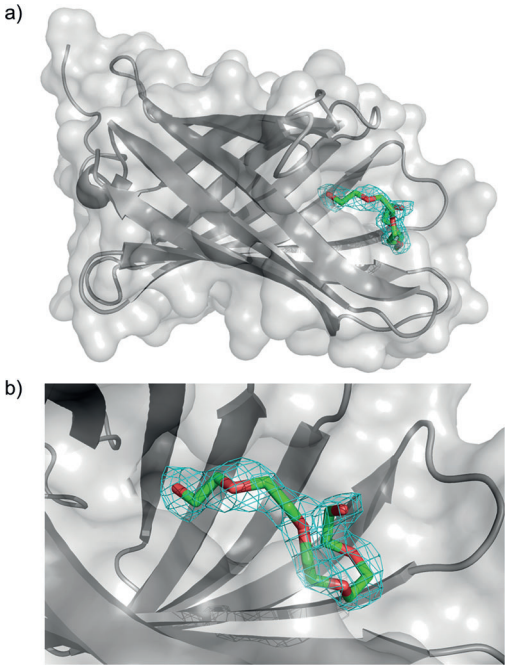

Figure 4. Crystal structure of NB4 at a 2.2 Å resolution. a) Whole structure and b) close-up views of the polyethylene glycol molecule within the cavity. The $2F_o$–F_c electron density (1.0 σ) is shown.

Table 1. Polymerization of phenylacetylene at 25 °C with determined *trans*/*cis* ratios and molecular weight distributions.[a]

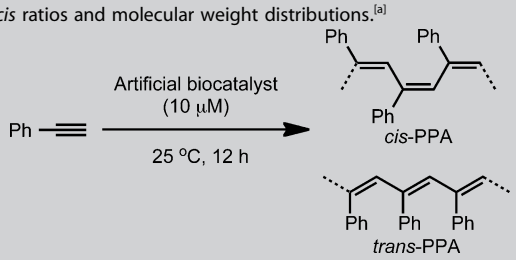

Entry	Hybrid biocatalyst	*trans*/*cis*[b]	M_n[c]	M_w/M_n[c]
1	Mb(A125C)-**Rh**	9:91	46 500	2.3
2	NB(Q96C)-**Rh**	54:46	42 800	2.1
3	NB1-**Rh**	44:56	36 500	2.6
4	NB2-**Rh**	45:55	38 300	2.2
5	NB3-**Rh**	55:45	36 800	2.2
6	NB4-**Rh**	82:18	38 900	2.4
7	NB5-**Rh**	77:23	38 300	2.3
8	NB6-**Rh**	39:61	38 300	2.4
9	NB7-**Rh**	34:66	31 100	2.5
10	NB8-**Rh**	28:78	31 500	2.4
11	NB9-**Rh**	40:60	34 600	2.1
12	NB10-**Rh**	22:78	38 600	2.7

[a] The polymerization of phenylacetylene was performed in the presence of the hybrid biocatalyst (10 μM) in a buffer (10 mM Tris-HCl, pH 8.0) under emulsion conditions for 12 h at 25 °C. The *trans*/*cis* ratio for 12 h was shown because the *trans* selectivity was decreased at 24 h probably because of the gradual unfolding of the protein during the polymerization. [b] Determined by ^{1}H NMR spectroscopy. [c] Determined by GPC in $CHCl_3$.

Polymerization of phenylacetylene

All emulsion polymerizations were performed with an identical hybrid catalyst (10 μM) and phenylacetylene (1 M) in Tris-HCl buffer solution (0.5 mL) at pH 8.0 and room temperature (25 °C) for 12 h (Table 1). After the polymerization, the reaction mixture was freeze-dried. The residue was washed with hexane and dried under vacuum to give PPA. The molecular weight (M_n) and the distribution (M_n/M_w) of PPA were determined by gel permeation chromatography (GPC). Chloroform was used as an eluent at a flow rate of 1.0 mL min^{-1} at 40 °C. The *trans*/*cis* ratio of PPA was determined by ^{1}H NMR spectroscopy (Figure S7). A hybrid biocatalyst, Mb(A125C)-**Rh**, was used as a reference. This protein has the covalently linked Rh complex on the surface of myoglobin and produces PPA with a high *cis* content (>91%; Table 1, entry 1). In contrast, NB(Q96C)-**Rh** harbors the Rh complex within the cavity of NB(Q96C) and yields PPA with a 54% *trans* content (Table 1, entry 2). The re-engineered hybrid biocatalysts (NB1-**Rh**, NB2-**Rh**, and NB3-**Rh**), each of which have an enlarged cavity as a result of an Ala replacement, were found to produce PPA with a moderate *trans* content of 44, 45, and 55%, respectively (Table 1, entries 3–5), which is similar to that of NB(Q96C)-**Rh** (Table 1, entry 2). These results indicate that the larger cavity does not enhance the *trans* selectivity in PPA production. It is interesting that NB4-**Rh** (in which two His residues are replaced with Leu residues) produces PPA with an 82% *trans* content, the highest among all the generated hybrid catalysts (Table 1, entry 6). The polymer produced by NB5-**Rh**, which has a cavity similar in size and shape to the cavity of NB4-**Rh** (Figure S2), produces PPA with a high *trans* content of 77% (Table 1, entry 7).

Selective phenylacetylene polymerization promoted by the hybrid biocatalysts with small cavities was also evaluated. The

hybrids, NB6-**Rh**, NB7-**Rh**, and NB8-**Rh**, have a partially crowded cavity and produce PPA with a low *trans* content (39, 34, and 28%; Table 1, entries 8–10). The Trp residue comes into contact with the Rh moiety in NB6-NB8-**Rh** and could interfere with monomer access to the catalytic center (Figure S8) to result in a decrease of the *trans* content. NB9-**Rh** and NB10-**Rh** also have a crowded cavity. These variants also produce PPA with a low *trans* content (40 and 22%; Table 1, entries 11 and 12). Consequently, NB5-**Rh** and NB4-**Rh** produced PPA with a high *trans* content because a large cavity enables the precise positioning of the Rh complex, which is a prerequisite to increase the *trans* content in PPA synthesis.

MD simulation

As the structural basis to model the hybrid biocatalysts, the X-ray structure of native NB (PDB: 2A13) and the NB variants (NB4, NB5, NB6, NB9, and NB10), the calculated structures of the NB variants (NB1, NB2, NB3, NB7, and NB8), and the high-resolution X-ray structure of the Rh complex were used. According to the procedure published previously,[14] the modeling was performed by using YASARA[20] Structure Version 13.6.16. Superimposed structures of NB1-**Rh**, NB4-**Rh**, and NB6-**Rh** are shown in Figure 5. The total energy of the Rh complex and the surrounding 14 amino acid residues are plotted against the distance between the Rh ion and the Cα atom of Leu75, which shows the conformational distribution of the Rh moiety within the cavity. The result of NB1-**Rh** clearly indicates the existence of two major conformations, which suggests the substantial flexibility of the Rh active site (Figure 5a). The NB1-**Rh** biocatalyst produces PPA with a low *trans* content. The decrease of the *trans* selectivity could be explained by uncontrolled access of the monomer owing to the flexibility of the Rh active site. The MD calculation also suggests that the Rh moiety possesses a defined orientation within the NB4 cavity (Figure 5b), which thereby provides a confined environment for the stereoselective polymerization of *trans*-PPA. Although the Rh moiety in NB6, which has a Trp residue, exhibits a narrowly distributed conformation, NB6-**Rh** produces PPA with a low *trans* content. The bulky Trp residue within the cavity might influence the access of the monomer to the Rh center (Figure 5c).

Conclusions

We re-engineered the cavity of Rh-complex-linked nitrobindin by computationally guided site-directed mutagenesis, which resulted in the identification of key residues that modulate and significantly improve the *trans*/*cis*-stereoselectivity in phenylacetylene polymerization. Particularly, the hybrid biocatalysts NB4-**Rh** (NB(H76L/Q96C/H158L)-**Rh**) and NB5-**Rh** (NB(F44W/H76L/Q96C/H158L)-**Rh**) yielded an inverted stereopreference for *trans*-polyphenylacetylene synthesis (up to 82% *trans*). X-ray crystal structure and molecular dynamics simulation results yielded molecular insights on how the stereopreference is guided within the hybrid catalysts and how monomer access to the Rh center is controlled.

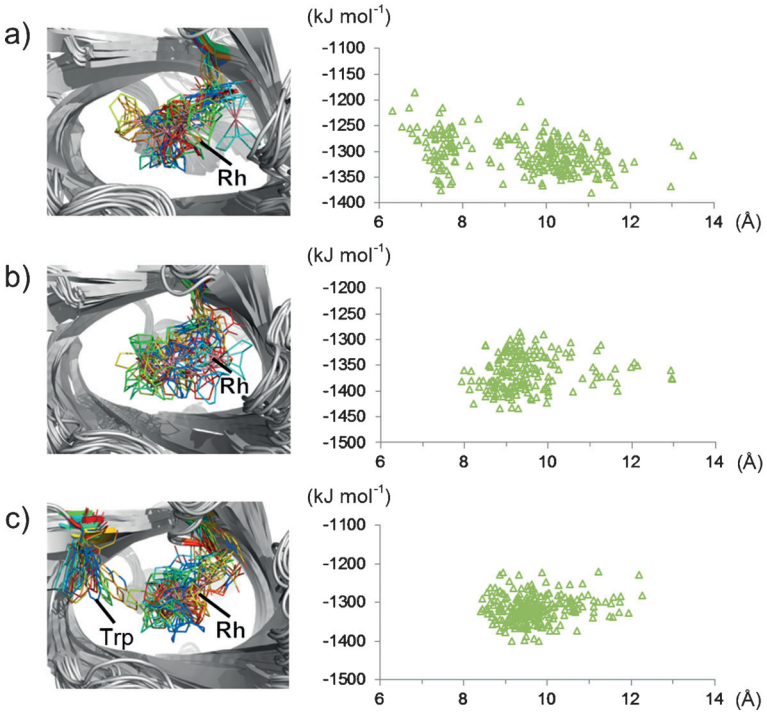

Figure 5. The distribution of the Rh complex within the cavity of a) NB1-**Rh**, b) NB4-**Rh**, and c) NB6-**Rh** during MD calculations at 298 K for 1500 ps. 16 selected snapshot structures are shown in rainbow colors (left), and the total energy of the Rh complex and the surrounding 14 amino acid residues (position 41, 44, 46, 75, 76, 96, 98, 100, 127, 128, 148, 150, 158, and 159) are plotted against the distance between the Rh ion and Cα of Leu75 (right). The total 240 minimized structures are plotted as green triangles.

Experimental Section

General

^{1}H NMR spectra were recorded by using a Bruker DPX400 NMR spectrometer. High-resolution magic angle spinning (HR-MAS) experiments were performed by using a Varian Unity Inova 600 MHz NMR spectrometer equipped with a 4 mm gHX Nanoprobe. ESI-TOF MS analysis was performed by using an Applied Biosystems Mariner API-TOF Workstation or a Bruker micrOTOF focus III mass spectrometer, and MALDI-TOF MS analysis was performed by using a Bruker autoflex III mass spectrometer. UV/Vis spectra were recorded by using a Shimadzu UV-3150 double-beam spectrophotometer and BioSpec-nano. Mutagenesis and amplification were performed by using a Bio-Rad PCR T100TM thermal cycler. The proteins were purified by using

a GE healthcare ÄKTA Purifier system at 4 °C. CD spectra were recorded by using a JASCO J720S spectrometer. ICP-OES was performed by using a Shimadzu ICPS-8100 emission spectrometer. pH values were monitored by using a Horiba F-52 pH meter. Air-sensitive procedures were performed in an MBraun glovebox. GPC was performed by using a TOSOH SC8020 apparatus with a refractive index detector using a TOSOH TSKgel G4000HHR column.

Subcloning of expression plasmids for NB variants

The NB(M75L/Q96C/M148L) gene with *Strep*-tag II was amplified as the pDEST14 plasmid that encoded the NB(M75L/Q96C/M148L) gene as a template. The forward primer that coded the *NdeI* restriction site and *Strep*-tag II gene:

5′-ATCTTACATATGTGGAGCCAC-CCGCAGTTCGAAAAAAAT CAACTGCAACAACTGCAAAATCCGGGC-3′

and the reverse primer that encoded the *XhoI* site:

5′-TGGTGCTCGAGCTATTACAGTTTGTCCAGGATGGCTTTCA-GGTGC-3′

were used. The polymerase chain reaction (PCR) product was digested with *NdeI* and *XhoI*, and subcloned into the pET42b(+) vector. The other expression plasmids for the NB variant were constructed according to the standard protocol of the QuickChangeII site-direct mutagenesis kit (Stratagene) by using the expression plasmids for NB(M75L/Q96C/M148L) as a template. The plasmids were amplified by PCR using *PfuUltra* High-Fidelity DNA Polymerase (Agilent Technologies), and the amplified plasmids were treated with DpnI restriction enzymes (Stratagene). The plasmids for the variant were transformed into DH5α competent cells. The forward and reverse primers used in this study are listed in Scheme S1.

Expression and purification of NB variants

The resulting expression plasmids that encode the NB variant gene with *Strep*-tag II were transformed into *E. coli* BL21 Star (DE3). Each 1.5 L of a Luria-Bertani medium that contained kanamycin (50 $\mu g\,mL^{-1}$) was inoculated with a 10 mL culture ($OD_{600} = 0.5 \sim 0.7$) of the transformed cells. The cells were shaken at 37 °C and 180 rpm until the OD_{600} of the culture reached approximately 0.5. Isopropyl-β-D-1-thiogalactopyranoside (IPTG) was added to a final concentration of 0.5 mM to induce the expression. The incubation was continued at 30 °C and 160 rpm for approximately 24 h. The cells were harvested by centrifugation at 12000 g for 9 min.

The harvested cells were resuspended in ≈100 mL of 100 mM Tris-HCl buffer (pH 8.0) that contained 1 mM EDTA, 150 mM NaCl, and 10 mM DTT. The cells were lysed by sonication (Branson Sonifier 250, 70% duty cycle, output = 6 cycles for 30 s). After centrifugation at 12000 g for 9 min, benzonase nuclease was added to the collected supernatant. The supernatant was loaded on a Strep-Tactin column (IBA, Germany), which was equilibrated in 100 mM Tris-HCl buffer (pH 8.0) that contained 1 mM EDTA and 150 mM NaCl. The target protein was collected in 100 mM Tris-HCl buffer (pH 8.0) that contained 1 mM EDTA, 150 mM NaCl, and 2.5 mM desthiobiotin. Furthermore, the protein was purified by using a HiTrap DEAE and benzamidine column (GE Healthcare) in 100 mM Tris-HCl buffer (pH 8.0) that contained 1 mM EDTA and 150 mM NaCl. The target protein was concentrated to approximately 1.0 mM by using an Amicon-stirred ultrafiltration cell with a 10 kDa molecular weight cutoff membrane (Millipore). The purified NB mutants were characterized by SDS-PAGE (Figure S1) and MALDI-TOF MS (Table S1).

Crystallization and structure analysis

The NB variants (NB5, NB6, NB9, and NB10) for the X-ray crystal structure analysis were crystallized by the hanging-drop vapor diffusion method at 293 K. The crystals were grown on siliconized coverslips by the equilibration of a mixture that contained 1.0 μL of the protein solution (1.0 mM protein in 5 mM MES buffer, pH 6.0, 200 mM NaCl, 1 mM dithioerythritol) and 1.0 μL of the reservoir solution (100 mM Tris-HCl buffer, pH 8.0, polyethylene glycol 2000 (18 ~ 20%)) with 100 μL of the reservoir solution (condition 1). The needle-shaped crystals of NB4-**Rh** and NB4 as a reference were obtained by the equilibration of a mixture that contained 2.0 μL of the protein solution (1.0 mM protein in 5 mM MES buffer, pH 6.0, 200 mM NaCl) and 2.0 μL of the reservoir solution (100 mM MES buffer, pH 6.5, polyethylene glycol 400 (26%)) with 100 μL of the reservoir solution at 293 K by using the hanging-drop vapor diffusion method (condition 2).

Crystals of NB5, NB6, NB9, and NB10 grown under the condition 1 were collected with a standard nylon loop, soaked in cryoprotectant solution (67% v/v Paraton-N, 28% v/v paraffin oil, 5% v/v glycerol), and flash-cooled in an N_2 gas stream at 100 K. Crystals of NB4-**Rh** and NB4 grown under the condition 2 were collected and directly flash-cooled in the N_2 gas stream. The X-ray diffraction data were collected at SPring-8 BL44XU or by using our in-house system.

The data were integrated and scaled by using the program HKL2000[21] and further processed by using the CCP4 software package.[22] The initial phases were obtained by the molecular replacement method by using the program PHASER.[23] The reported structure of NB (PDB code 2A13) was used as a search model. The model was refined with multiple rounds of manual rebuilding by using COOT[24] and crystallographic refinement by REFMAC5.[25] The data collection and refinement statistics are summarized in Table S3. Figures that depict the structures were prepared by using PYMOL (http://www.pymol.org). The atomic coordinates and structure factors were deposited in the Protein Data Bank (http://www.rcsb.org/PDB codes: 3WJB for NB4, 3WJC for NB4-**Rh**, 3WJD for NB5, 3WJE for NB6, 3WJF for NB9, and 3WJG for NB10).

MD simulation

The modeling was performed by using YASARA[20] Structure Version 13.6.16 that employed force field AMBER03[26] for protein residues and GAFF[27] using AM1/BCC[28] partial charges for the catalyst covalently bound to Cys96. The metal was replaced by Co as no parameters were available for Rh. To maintain the correct coordination geometry, the distances from the metal to all five C atoms of the Cp ligand were constrained to 2.2 Å and the η^5 coordination was represented by five force field arrows. To maintain η^2 coordination of the COD ligand, four force field arrows were defined and the distances were constrained to 2.0 Å, according to the X-ray structure of the Rh complex. The partial charge of the metal was set to +1 and the total charge of the Rh complex was set to zero. The bond orders for the Cp ligand were defined as 1.67 Å to maintain an aromatic system. The Rh complex was placed manually in the cavity adjacent to Cys96, and a bond was defined from the Cys S atom to the C1 or C2 atom of the maleimide group. The constructed hybrid catalysts were solvated in a box of TIP3P water molecules by using periodic boundaries at pH 7 and a density of 0.997 g mL^{-1}. Four starting structures that represent the cysteine–maleimide linker isomers were analyzed, and favorable models were identified for the covalent attachment to the reactive maleimide atoms C1 and C2 by simulated annealing and steepest descent minimization. The preminimized structures were relaxed by using MD calculations at 298 K for 1500 ps, and snapshots were taken at 25 ps intervals to analyze the binding modes. Each snapshot was minimized to 0 K by simulated annealing and steepest descent minimization, and then the total energy [kJ mol^{-1}] of the 14 specific amino acids (positions 41, 44, 46, 75, 76, 96, 98, 100, 127, 128, 148, 150, 158, and 159) and the Rh complex in each minimized structure were analyzed (Figures S8–S11).

Acknowledgements

This work was financially supported by a Japan–German Graduate Externship Program funded by JSPS, and a program entitled "Selectivity in Chemo- and Biocatalysts (SeleCa)" administered by DFG, MEXT Japan (A.O. and T.H.). We thank Dr. Kyoko Inoue for technical assistance during the NMR measurements as well as Dr. Takashi Tsujimoto and Prof. Hiroshi Uyama for their assistance with GPC measurements at the Department of Applied Chemistry, Graduate School of Engineering, Osaka University, and the staff for their excellent support during data collection on the BL44XU at SPring-8.

Keywords: biocatalysis · molecular dynamics · polymerization · protein engineering · rhodium

[1] a) Y. Lu, N. Yeung, N. Sieracki, N. M. Marshall, *Nature* **2009**, *460*, 855–862; b) M. T. Reetz, M. Rentzsch, A. Pletsch, M. Maywald, P. Maiwald, J. J.-P. Peyralans, A. Maichele, Y. Fu, N. Jiao, F. Hollmann, R. Mondière, A. Taglieber, *Tetrahedron* **2007**, *63*, 6404–6414; c) T. Heinisch, T. R. Ward, *Curr. Opin. Chem. Biol.* **2010**, *14*, 184–199; d) T. R. Ward, *Acc. Chem. Res.* **2011**, *44*, 47–57; e) P. J. Deuss, R. den Heeten, W. Laan, P. C. J. Kamer, *Chem. Eur. J.* **2011**, *17*, 4680–4698; f) T. Ueno, H. Tabe, Y. Tanaka, *Chem. Asian J.* **2013**, *8*, 1646–1660; g) T. Hayashi, Y. Hisaeda, *Acc. Chem. Res.* **2002**, *35*, 35–43; h) *Bio-inspired Catalysts* (Ed.: T. R. Ward), Springer, Heidelberg, **2009**.

[2] a) M. Ohashi, T. Koshiyama, T. Ueno, M. Yanase, H. Fujii, Y. Watanabe, *Angew. Chem.* **2003**, *115*, 1035–1038; *Angew. Chem. Int. Ed.* **2003**, *42*, 1005–1008; b) A. Mahammed, Z. Gross, *J. Am. Chem. Soc.* **2005**, *127*, 2883–2887; c) Q. Jing, K. Okrasa, R. J. Kazlauskas, *Chem. Eur. J.* **2009**, *15*, 1370–1376; d) Y. Sano, A. Onoda, T. Hayashi, *Chem. Commun.* **2011**, *47*, 8229–8231; e) T. Matsuo, A. Hayashi, M. Abe, T. Matsuda, Y. Hisaeda, T. Hayashi, *J. Am. Chem. Soc.* **2009**, *131*, 15124–15125; f) T. Matsuo, K. Fukumoto, T. Watanabe, T. Hayashi, *Chem. Asian J.* **2011**, *6*, 2491–2499; g) F. W. Monnard, E. S. Nogueira, T. Heinisch, T. Schirmer, T. R. Ward, *Chem. Sci.* **2013**, *4*, 3269–3274; h) J. Podtetenieff, A. Taglieber, E. Bill, E. J. Reijerse, M. T. Reetz, *Angew. Chem.* **2010**, *122*, 5277–5281; *Angew. Chem. Int. Ed.* **2010**, *49*, 5151–5155; i) Z. T. Ball, *Acc. Chem. Res.* **2013**, *46*, 560–570.

[3] a) M. E. Wilson, G. M. Whitesides, *J. Am. Chem. Soc.* **1978**, *100*, 306–307; b) J. Collot, J. Gradinaru, N. Humbert, M. Skander, A. Zocchi, T. R. Ward, *J. Am. Chem. Soc.* **2003**, *125*, 9030–9031; c) H. Yamaguchi, T. Hirano, H. Kiminami, D. Taura, A. Harada, *Org. Biomol. Chem.* **2006**, *4*, 3571–3573; d) M. T. Reetz, J. J.-P. Peyralans, A. Maichele, Y. Fu, M. Maywald, *Chem. Commun.* **2006**, 4318–4320.

[4] a) H. L. Levine, E. T. Kaiser, *J. Am. Chem. Soc.* **1978**, *100*, 7670–7677; b) Z.-P. Wu, D. Hilvert, *J. Am. Chem. Soc.* **1989**, *111*, 4513–4514; c) D. Qi, C.-M. Tann, D. Haring, M. D. Distefano, *Chem. Rev.* **2001**, *101*, 3081–3111; d) M. T. Reetz, M. Rentzsch, A. Pletsch, M. Maywald, *Chimia* **2002**, *56*, 721–723; e) J. R. Carey, S. K. Ma, T. D. Pfister, D. K. Garner, H. K. Kim, J. A. Abramite, Z. Wang, Z. Guo, Y. Lu, *J. Am. Chem. Soc.* **2004**, *126*, 10812–10813; f) T. Matsuo, C. Imai, T. Yoshida, T. Saito, T. Hayashi, S. Hirota, *Chem. Commun.* **2012**, *48*, 1662–1664; g) P. Haquette, B. Talbi, L. Barilleau, N. Madern, C. Fosse, M. Salmain, *Org. Biomol. Chem.* **2011**, *9*, 5720–5727; h) F. Philippart, M. Arlt, S. Gotzen, S.-J. Tenne, M. Bocola, H.-H. Chen, L. Zhu, U. Schwaneberg, J. Okuda, *Chem. Eur. J.* **2013**, *19*, 13865–13871; i) J. Bos, A. García-Herraiz, G. Roelfes, *Chem. Sci.* **2013**, *4*, 3578–3582.

[5] J. M. Zimbron, T. Heinisch, M. Schmid, D. Hamels, E. S. Nogueira, T. Schirmer, T. R. Ward, *J. Am. Chem. Soc.* **2013**, *135*, 5384–5388.

[6] a) M. T. Reetz, N. Jiao, *Angew. Chem.* **2006**, *118*, 2476–2479; *Angew. Chem. Int. Ed.* **2006**, *45*, 2416–2419; b) J. Bos, F. Fusetti, A. J. M. Driessen, G. Roelfes, *Angew. Chem.* **2012**, *124*, 7590–7593; *Angew. Chem. Int. Ed.* **2012**, *51*, 7472–7475.

[7] a) T. Ueno, T. Koshiyama, M. Ohashi, K. Kondo, M. Kono, A. Suzuki, T. Yamane, Y. Watanabe, *J. Am. Chem. Soc.* **2005**, *127*, 6556–6562; b) A. Pordea, M. Creus, J. Panek, C. Duboc, D. Mathis, M. Novic, T. R. Ward, *J. Am. Chem. Soc.* **2008**, *130*, 8085–8088.

[8] T. K. Hyster, L. Knörr, T. R. Ward, T. Rovis, *Science* **2012**, *338*, 500–503.

[9] M. Creus, T. R. Ward, *Org. Biomol. Chem.* **2007**, *5*, 1835–1844.

[10] a) A. J. Heeger, *Angew. Chem.* **2001**, *113*, 2660–2682; *Angew. Chem. Int. Ed.* **2001**, *40*, 2591–2611; b) A. G. MacDiarmid, *Angew. Chem.* **2001**, *113*, 2649–2659; *Angew. Chem. Int. Ed.* **2001**, *40*, 2581–2590; c) H. Shirakawa, *Angew. Chem.* **2001**, *113*, 2642–2648; *Angew. Chem. Int. Ed.* **2001**, *40*, 2574–2580; d) J. Liu, J. W. Y. Lam, B. Z. Tang, *Chem. Rev.* **2009**, *109*, 5799–5867.

[11] a) Z. Ke, S. Abe, T. Ueno, K. Morokuma, *J. Am. Chem. Soc.* **2011**, *133*, 7926–7941; b) B. Z. Tang, W. H. Poon, S. M. Leung, W. H. Leung, H. Peng, *Macromolecules* **1997**, *30*, 2209–2212; c) T. Ikariya, Y. Kishimoto, P. Eckerle, T. Miyatake, M. Kainosho, A. Ono, R. Noyori, *J. Am. Chem. Soc.* **1999**, *121*, 12035–12044.

[12] a) S. Abe, K. Hirata, T. Ueno, K. Morino, N. Shimizu, M. Yamamoto, M. Takata, E. Yashima, Y. Watanabe, *J. Am. Chem. Soc.* **2009**, *131*, 6958–6960; b) Z. Ke, S. Abe, T. Ueno, K. Morokuma, *J. Am. Chem. Soc.* **2012**, *134*, 15418–15429.

[13] C. M. Bianchetti, G. C. Blouin, E. Bitto, J. S. Olson, G. N. Phillips, Jr., *Proteins* **2010**, *78*, 917–931.

[14] A. Onoda, K. Fukumoto, M. Arlt, M. Bocola, U. Schwaneberg, T. Hayashi, *Chem. Commun.* **2012**, *48*, 9756–9758.

[15] The apo-NB variant, M75L/Q96C/M145L, a prototype protein of the present work, is abbreviated as NB(Q96C).

[16] J. Van Durme, J. Delgado, F. Stricher, L. Serrano, J. Schymkowitz, F. Rousseau, *Bioinformatics* **2011**, *27*, 1711–1712.

[17] a) D. G. Levitt, L. J. Banaszak, *J. Mol. Graphics* **1992**, *10*, 229–234; b) M. Hendlich, F. Rippmann, G. Barnickel, *J. Mol. Graphics Modell. J. Mol. Graphics Mod.* **1997**, *15*, 359–363; c) A. T. R. Laurie, R. M. Jackson, *Bioinformatics* **2005**, *21*, 1908–1916.

[18] The anchoring of the Rh complex within the NB variants from NB1–NB5 proceeded smoothly with good conversion, whereas the anchoring reactions of the NB variants from NB6–NB10, which contain the bulky Trp

residue were slower and produced a lower yield of the Rh complex (approximately 60%).
[19] The F_o–F_c omit map also confirms the covalent linkage between the Cys96 residue and the maleimide group of the Rh complex.
[20] E. Krieger, T. Darden, S. Nabuurs, A. Finkelstein, G. Vriend, *Proteins* **2004**, *57*, 678–683.
[21] Z. Otwinowski, W. Minor, *Methods Enzymol.* **1997**, *276*, 307–326.
[22] M. D. Winn, C. C. Ballard, K. D. Cowtan, E. J. Dodson, P. Emsley, P. R. Evans, R. M. Keegan, E. B. Krissinel, A. G. W. Leslie, A. McCoy, S. J. McNicholas, G. N. Murshudov, N. S. Pannu, E. A. Potterton, H. R. Powell, R. J. Read, A. Vagin, K. S. Wilson, *Acta Crystallogr. Sect. D* **2011**, *67*, 235–242.
[23] A. J. McCoy, R. W. Grosse-Kunstleve, P. D. Adams, M. D. Winn, L. C. Storoni, R. J. Read, *J. Appl. Crystallogr.* **2007**, *40*, 658–674.
[24] P. Emsley, K. Cowtan, *Acta Crystallogr. Sect. D* **2004**, *60*, 2126–2132.
[25] G. N. Murshudov, P. Skubak, A. A. Lebedev, N. S. Pannu, R. A. Steiner, R. A. Nicholls, M. D. Winn, F. Long, A. A. Vagin, *Acta Crystallogr. Sect. D* **2011**, *67*, 355–367.
[26] Y. Duan, C. Wu, S. Chowdhury, M. C. Lee, G. Xiong, W. Zhang, R. Yang, P. Cieplak, R. Luo, T. Lee, J. Caldwell, J. Wang, P. Kollman, *J. Comput. Chem.* **2003**, *24*, 1999–2012.
[27] J. Wang, R. M. Wolf, J. W. Caldwell, P. A. Kollman, D. A. Case, *J. Comput. Chem.* **2004**, *25*, 1157–1174.
[28] A. Jakalian, D. B. Jack, C. I. Bayly, *J. Comput. Chem.* **2002**, *23*, 1623–1641.

Received: December 10, 2013
Published online on ■■ ■■, 0000

*K. Fukumoto, A. Onoda, E. Mizohata, M. Bocola, T. Inoue, U. Schwaneberg, T. Hayashi**

■■ – ■■

Rhodium-Complex-Linked Hybrid Biocatalyst: Stereo-Controlled Phenylacetylene Polymerization within an Engineered Protein Cavity

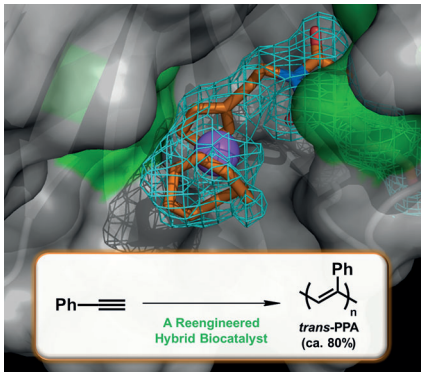

Hybrid biocatalysis, β in a barrel: The incorporation of a Rh complex into the cavity of the nitrobindin β-barrel scaffold through a covalent linkage provides a hybrid catalyst that promotes the polymerization of phenylacetylene. The appropriate structural optimization of the cavity by mutagenesis enhances the *trans* content of the polymer. PPA = Polyphenylacetylene.